

Alma Mater Studiorum Università di Bologna
Archivio istituzionale della ricerca

Decoding of standard and non-standard visuomotor associations from parietal cortex

This is the final peer-reviewed author's accepted manuscript (postprint) of the following publication:

Published Version:

Filippini M., Morris A.P., Breveglieri R., Hadjidimitrakis K., Fattori P. (2020). Decoding of standard and non-standard visuomotor associations from parietal cortex. JOURNAL OF NEURAL ENGINEERING, 17(4), 1-15 [10.1088/1741-2552/aba87e].

Availability:

This version is available at: <https://hdl.handle.net/11585/789028> since: 2021-01-16

Published:

DOI: <http://doi.org/10.1088/1741-2552/aba87e>

Terms of use:

Some rights reserved. The terms and conditions for the reuse of this version of the manuscript are specified in the publishing policy. For all terms of use and more information see the publisher's website.

This item was downloaded from IRIS Università di Bologna (<https://cris.unibo.it/>).
When citing, please refer to the published version.

(Article begins on next page)

ACCEPTED MANUSCRIPT

Decoding of standard and non-standard visuomotor associations from parietal cortex.

To cite this article before publication: Matteo Filippini *et al* 2020 *J. Neural Eng.* in press <https://doi.org/10.1088/1741-2552/aba87e>

Manuscript version: Accepted Manuscript

Accepted Manuscript is "the version of the article accepted for publication including all changes made as a result of the peer review process, and which may also include the addition to the article by IOP Publishing of a header, an article ID, a cover sheet and/or an 'Accepted Manuscript' watermark, but excluding any other editing, typesetting or other changes made by IOP Publishing and/or its licensors"

This Accepted Manuscript is © 2020 IOP Publishing Ltd.

During the embargo period (the 12 month period from the publication of the Version of Record of this article), the Accepted Manuscript is fully protected by copyright and cannot be reused or reposted elsewhere.

As the Version of Record of this article is going to be / has been published on a subscription basis, this Accepted Manuscript is available for reuse under a CC BY-NC-ND 3.0 licence after the 12 month embargo period.

After the embargo period, everyone is permitted to use copy and redistribute this article for non-commercial purposes only, provided that they adhere to all the terms of the licence <https://creativecommons.org/licenses/by-nc-nd/3.0>

Although reasonable endeavours have been taken to obtain all necessary permissions from third parties to include their copyrighted content within this article, their full citation and copyright line may not be present in this Accepted Manuscript version. Before using any content from this article, please refer to the Version of Record on IOPscience once published for full citation and copyright details, as permissions will likely be required. All third party content is fully copyright protected, unless specifically stated otherwise in the figure caption in the Version of Record.

View the [article online](#) for updates and enhancements.

Decoding of standard and non-standard visuomotor associations from parietal cortex.

M. FILIPPINI¹², A.P. MORRIS³, R. BREVEGLIERI¹, K. HADJIDIMITRAKIS^{1,3*}, P. FATTORI^{12*};

¹University of Bologna, Department of Biomedical and Neuromotor Sciences, Bologna, Italy;

² ALMA-AI: Alma Mater Research Institute for Human-Centered Artificial Intelligence

³Neuroscience Program, Biomedicine Discovery Institute, Department of Physiology, Monash University, Clayton, Australia

* Equal senior authors

Correspondence:

Dr. Matteo Filippini, Ph.D,

Department of Biomedical and Neuromotor Sciences,

University of Bologna, Piazza di Porta San Donato 2,

Bologna 40126, Italy E-mail: matteo.filippini7@unibo.it

Abstract

Objective

Neural signals can be decoded and used to move neural prostheses with the purpose of restoring motor function in patients with mobility impairments. Such patients typically have intact eye movement control and visual function, suggesting that cortical visuospatial signals could be used to guide external devices. Neurons in parietal cortex mediate sensory-motor transformations, encode the spatial coordinates for reaching goals, hand position and movements, and other spatial variables. We studied how spatial information is represented at the population level, and the possibility to decode not only the position of visual targets and the plans to reach them, but also conditional, non-spatial motor responses.

Approach

The animals first fixated one of nine targets in 3D space and then, after the target changed color, either reached toward it, or performed a non-spatial motor response (lift hand from a button). Spiking activity of parietal neurons was recorded in monkeys during two tasks. We then decoded different task related parameters.

Main results

We first show that a maximum-likelihood estimation (MLE) algorithm trained separately in each task transformed neural activity into accurate metric predictions of target location. Furthermore, by combining MLE with a Naïve Bayes classifier, we decoded the monkey's motor intention (reach or hand lift) and the different phases of the tasks. These results show that, although V6A encodes the spatial location of a target during a delay period, the signals they carry are updated around the movement execution in an intention/motor specific way.

Significance

1
2
3 52 These findings show the presence of multiple levels of information in parietal cortex that could be decoded
4
5 53 and used in brain machine interfaces to control both goal-directed movements and more cognitive
6
7 54 visuomotor associations.
8
9

10 55
11
12 56
13
14 57 **Keywords**

15
16 58 Reaching, brain computer interfaces, decoding, electrophysiology, posterior parietal cortex, monkey
17
18
19 59

20
21
22 60 **1. Introduction**

23
24 61 A large body of evidence shows that motor intentions can be decoded from neural activity and used to control
25
26 62 artificial limbs (1–6). In most of these cases, neural activity was recorded from motor cortex, where signals
27
28 63 are highly correlated with desired movement trajectories (1,3). An alternative approach is to exploit signals
29
30 64 earlier in the sensorimotor pathways, particularly in posterior parietal cortex (PPC), where neurons are
31
32 65 sensitive to movement parameters and more abstract representations of intention and visuospatial attention
33
34 66 (7–13). The spatial target of a reach, for example, can be decoded from a small number of neurons in PPC in
35
36 67 monkeys (14–17), and from fMRI signals (18,19) or intracortical signals (2) in humans.
37
38
39

40 68
41
42 69 A device that relies on signals from PPC, rather than from motor cortex, has the potential advantage that it
43
44 70 could (also) infer the intended outcome of an action rather than the kinematics of a specific movement. This
45
46 71 could provide greater flexibility in its use across a range of assistive technologies. However, PPC signals are
47
48 72 multi-modal and high-dimensional (8,20,21), making difficult to disentangle between these signals.
49
50
51 73

52
53 74 Here, we tested whether multiple task- and intention-related variables could be decoded simultaneously
54
55 75 from population activity in area V6A, located in the posterior parietal cortex (PPC) (22,23). V6A neurons are
56
57 76 involved in both reaching and grasping (24–27), and are tuned for kinematic parameters such as direction
58
59 77 (28,29) and amplitude of hand movement (24). In addition, they encode visual target location in 3D in the
60

1
2
3 78 absence of reaching (27,30–32), thus enabling the use of visuospatial information in task contexts where no
4
5 79 arm movement is planned.
6

7
8 80

9
10 81 To test this hypothesis, we decoded neural activity recorded from area V6A in macaques while they
11
12 82 performed sequentially two sensorimotor tasks (Fig. 1). Both tasks required fixation of a visual target that
13
14 83 varied position in 3D space across trials, but they differed in the type of motor response required: a reach
15
16 84 movement towards the target (fixate-to-reach task), or a non-spatial motor response (fixate-to-hand lift task)
17
18 85 that was instructed by the color code of the target, but not directed towards it. We used a Maximum
19
20
21 86 Likelihood Estimator (MLE) that permits a metric estimation of the target position.
22

23 87 We then compared population codes between the two tasks during the delay period. At the single neuron
24
25 88 level, we recently reported that the most represented type of V6A cells (44%) showed different firing
26
27 89 between these two tasks (33), so we expected that the population signals would be different. In addition, we
28
29
30 90 looked for activity patterns related to distinct task stages and how they gradually evolved to support the
31
32 91 movement. These switches can be useful to trigger prosthesis movement (17,34).
33

34 92 We found that we could reliably decode: target position, type of intended movement and different cognitive
35
36 93 states from the very same population of neurons. At the same time, generalization analysis across tasks
37
38 94 showed that the neural codes were very similar in most task phases and diverged only immediately before
39
40 95 the movement onset. The finding that multiple variables and types of motor responses were coded
41
42 96 dynamically in the same brain area could be exploited for neuroprosthetic applications.
43
44
45

46 97

47 48 98 **2. Methods**

49

50
51 99

52
53 100 The experimental part of this study was performed in accordance with the guidelines of the EU Directives
54
55 101 (86/609/EEC; 2010/63/EU) and the Italian national law (D.L. 116-92, D.L. 26-2014) on the use of animals in
56
57 102 scientific research. Protocols were approved by the Animal-Welfare Body of the University of Bologna. During
58
59
60

1
2
3 103 training and recording sessions, particular attention was paid to any behavioral and clinical sign of pain or
4
5 104 distress.
6
7 105
8
9 106
10
11
12 107 *2.1 Experimental Procedures*
13
14 108
15
16 109 Two male macaque monkeys (*Macaca fascicularis*) weighing 4.4 kg (Monkey 1, M1) and 3.8 kg (Monkey 2,
17
18 M2) were used. Single cell activity was recorded extracellularly by means of single electrode from the anterior
19 110
20 bank of the parieto-occipital sulcus (POs). We performed multiple electrode penetrations using a five-channel
21 111
22 multielectrode recording system that permitted to record from up to five single electrodes at once (Thomas
23 112
24 Recording GmbH, Giessen, Germany). We recorded the activity of 162 V6A (36) neurons, 100 cells from M1
25 113
26 and 62 cells from M2. Although five electrodes was the maximum number of our recording system, on
27 114
28 average we were recording from 2-3 neurons at once; in total, the number of sessions distributed between
29 115
30 M1 and M2 was 45 (22 + 23). Action potentials (spikes) in each channel were isolated with a waveform
31 116
32 discriminator (Multi Spike Detector; Alpha Omega Engineering Nazareth, Israel) and were sampled at 100
33 117
34 kHz. Quality of single-unit isolation was determined by the homogeneity of spike wave forms and clear
35 118
36 refractory periods in ISI histograms during spike-sorting. Only well-isolated units not changing across tasks
37 119
38 were considered. The experimental procedures are described in full detail in Breveglieri et al. (2014).
39 120
40
41 121
42
43 122 *2.2 Behavioral Tasks*
44
45
46 123
47
48 124 Electrophysiological signals were collected while the monkeys were performing two instructed-delay tasks:
49
50 a fixate-to-reach task (fix-reach) and a fixate-to-lift hand task (fix-lift), as illustrated in Figure 1. In both tasks,
51 125
52 one of nine targets placed in several locations in 3-D space was switched on and the animal had to fixate it
53 126
54 and, when instructed (target color change), either perform a reach toward the target (fix-reach), or lift the
55 127
56 hand from the home button (fix-lift). Monkeys sat in a primate chair, with the head restrained, and faced a
57 128
58
59
60

horizontal panel located at eye level. Nine light-emitting diodes (LEDs) mounted on the panel at different distances from the eyes were used as fixation and reaching targets (Figure 1A, left). As shown in the right part of Figure 1A, the nine target LEDs were arranged in a radial grid consisting of three directions: version angles of -15° , 0° , and $+15^\circ$ and three depths i.e., vergence angles of 17.1° , 11.4° , and 6.9° . The two animals had the same interocular distance (3.0 cm), so we placed the grid at the same distance from the monkeys in both animals (nearest targets: 10 cm; intermediate targets: 15 cm; far targets: 25 cm). The range of vergence angles was chosen to be within the limits of peripersonal space, so the monkeys were able to reach all target positions. The animals performed the tasks with the arm contralateral to the recording site. The two tasks were performed in separate blocks. In case of fix-lift task, a plexiglass barrier prevented the hand movement toward the target.

In both tasks, the animal initiated a trial by pressing and holding a home button (HB; 2.5 cm in diameter, Figure 2A) placed 5 cm in front of the torso, outside the field of view (FREE epoch). After a delay of 1000 ms, one of the nine LEDs was turned on in green, cuing the animal to initiate fixation. After a delay of 1700–2500 ms (DELAY epoch), the LED changed to red, cuing the animal to either perform a reach to the target (fix-reach task) or to simply release the button (fix-lift task) (MOV epoch). In the case of fix-reach task, monkeys had 1 sec after the go signal to reach the target, otherwise the trial was aborted. Then, monkeys pressed the target and held the hand on it for 800–1200 ms. The target offset cued the monkeys to release the LED and return to the home button, which ended the trial and allowed monkeys to receive reward. In the case of fix-lift task, monkeys had 1 s to release the button to have the reward.

Only correctly executed trials were used in this analysis. We collected 10 correct trials for each of the 9 conditions (targets) and for each tested task.

2.3 Data Analysis

2.3.1 Preprocessing.

Neurons activities were analyzed as spike counts within single trials. The spike times on each trial were counted within a 100-ms window that stepped in 100 ms increments. Because these neurons

1
2
3 155 were not recorded simultaneously, a “trial” in this context refers to a synthetic dataset in which a single
4
5 156 experimental trial was drawn randomly for each neuron from a common behavioral condition and collated.
6
7
8 157 This is a common and useful way to simulate population codes in the brain from single neuron data (37–40).
9
10 158 It should be noted, however, that this approach ignores potential effects of correlated spike-count variability
11
12 159 on the coding of target position.
13

14 160
15
16 161 2.3.2 Population Decoding. To decode the different parameters which describes the fix-reach or the fix-lift
17
18 task, two different decoding algorithms were used in our analysis: a Maximum Likelihood Estimator (MLE)
19 162 and a Naïve Bayes classifier (NB). Metric estimation of target positions (in a 2D grid) relied on MLE decoding
20
21 163 algorithm. This algorithm was used successfully to decode eye position signals from macaque parietal and
22
23 164 temporal cortex (37,38). We adapted this implementation to our motor task using signals from area V6A. In
24
25 165 addition to the decoding of the target spatial position, we examined two additional parameters: given a
26
27 random bin of activity, whether it was possible to predict the current task type (fix-reach or fix-lift) and the
28 166 current task phase (epoch free, or delay, or movement, see below). These latter parameters, together with
29
30 167 metric estimation of target location provide a detailed snapshot of the ongoing action. In particular, we
31
32 168 combined the MLE and NB decoders to recognize whether the monkey performed a reach toward the target
33
34 or simply lifted his hand off the button. Decoding of task phase was performed using a simple NB
35
36 169 implementation to identify the different epochs of tasks.
37 170
38
39 171
40
41 172
42

43 173
44
45 174 2.3.3 Target decoding. MLE decoder estimated the spatial coordinates of targets given the population neural
46
47 activity. The implementation is described in full detail in Morris et al. (37,38): here are summarized the key
48 175 steps. A regression surface (second order polynomial, eq.1 and a real example in Fig.2A) was calculated for
49
50 176 each neuron and it was used to estimate the effect of target position (*direction* X , *depth* Y) on mean spike
51
52 177 counts (\hat{c}).
53
54 178
55

56
57 179 Eq. 1 $\hat{c}(X, Y) = a_0 + a_1X + a_2Y + a_3X^2 + a_4Y^2 + a_5XY$
58
59
60

Assuming Poisson statistics, eq.1 becomes a description of how both the mean and variance (both equal to λ) of spike counts varied as a function of target position. Thus, conditional probability over spike counts for a given target position (x,y) was:

$$\hat{p}(C|x,y) = \text{Poisson}[\lambda(x,y)] \text{ where } \lambda(x,y) = \hat{c}(x,y)$$

Equation 2 provides a critical quantitative link between target position and the neural response: the probability of a neural response given a target position (in statistical terms, a “likelihood function”); but without additional steps, they do not provide the information needed for decoding. Decoding implements the reverse direction of inference, so it requires an estimate of the probability of each target position given an observed spike count (i.e. $p(X,Y|c)$, the posterior probability distribution (Fig. 2B). These two types of conditional probability are related via the Bayes rule. Assuming statistical independence among N neurons, the optimal way to combine posterior probability density functions across the population is to take their product, which is usually implemented as a sum of their logarithms. As the final step, the eye position associated with the maximum a posteriori (MAP) log-likelihood (i.e., the MAP estimate) in $\log p(X,Y|C \text{ population})$ was selected as the point estimate for target direction and depth (Fig. 2C). To assess the ability of our model to predict the correct target positions, we used a R^2 metric, R^2 is the proportion of the variance in the dependent variable (x,y of targets) that is predictable from the independent variable (decoded spike counts). Accuracy was evaluated as the Euclidean distance from the mean of predictions (over cross-validation) to the real target position. Similarly, precision was computed as distance from predictions to the mean of predictions for a given target position.

2.3.4. Task type decoding. To identify which task the monkey executed, i.e. fix-reach or fix-lift, we used a combination of the MLE decoder used for target decoding and a Bayesian classifier. In this case we were not interested to predict the target position, so the analysis was conducted pooling together spike counts from different positions but keeping separate the data of the two tasks. First, a regression surface for each neuron was calculated in the same way as the method proposed above. Second, residuals from surface fitting were used to train a NB classifier to discriminate between tasks. Residuals are a common way to express the

distance between the model resulting from the fitting and the real data. Deviations from the model can be used as feature for machine learning algorithms, in the way that they are very informative about the uncommon part between the two datasets. Since we wanted to solve a simple binary classification problem between two classes (i.e. given the spike count of any bin taken in the interval of one of the two tasks predict which task it belonged to) we adopted a Naïve Bayesian classifier. Keeping the assumption of independence between features, Naive Bayesian classifiers are robust, fast and widely used as neural decoders in case the goal is to classify discrete quantities as neural states can be. Matlab '*ClassificationNaiveBayes*' class implementation was used. Results are given as recognition rate computed from a 50-fold cross-validation. Such cross-validation was used to keep the analysis fair compared to the others where fewer trials were available; here 90 trials per class were available and keeping out 3 trials for testing per cross-validation iteration seemed a good compromise.

2.3.5. Task phase decoding. To test whether the spike counts (100ms bin) contained information about the different task phases, we trained a NB classifier to discriminate between the three FREE, DELAY and MOVEMENT states (see 2.2 for behavioral epochs). Simple spike counts were used to build-up the population feature vectors with dimension n neurons by 10 trials \times 9 conditions \times 3 states (270 vectors). The three states correspond to three classes for the classifier. A leave one out cross-validation over 10 trials was used. A custom Python script based on *scikit-learn* implementation of Naïve Bayes classifier with a Poisson assumption was used (41). Results are reported as probability for each state along the time (Fig. 7A) and confusion matrices (Fig. 7B).

2.3.6 Cross-validation. Leave-One-Out (LOO) cross-validation was used to ensure that the results of population decoding reflected reliable characteristics of the neural code for target position and not effects of overfitting. For each cross-validation set, the spike counts at each of the 9 target positions and the associated regression coefficients were estimated from 90% of the available trials for each neuron ("training set"). Decoding was then performed on 100 synthetic trials (see 2.3.1) drawn at random from the remaining

trial for each neuron. Unless otherwise stated, the population decoding results presented herein were therefore derived from 900 synthetic trials (100 test trials for each cross-validation sets).

2.3.7 Generalization. In order to compare neural activation patterns under different experimental paradigm we can build models (training the algorithm) on neural data from a specific task, then using data from the other task to make predictions. Prediction accuracy (expected vs predicted) represents metric for the grade of similarity between codes. Given the example for training on fix-reach and testing on fix-lift task, we computed the regression surfaces with spike counts from fix-reach task.

3. Results

Two monkeys were trained to perform in randomized block sequence the fix-reach and the fix-lift task. Fixation and reach targets were nine touch-sensitive LEDs, placed in the 3-D space at three different directions (version angles -15° , 0° , $+15^\circ$) and three different distances (vergence angles, 17.1° , 11.4° and 6.9° ; Fig. 1A). The two tasks were identical except for the motor response (reaches vs. hand lifts; Fig.1B-C). Neurons were recorded from two macaque monkeys (see 2.1 for more details) and were included in the subsequent analyses, only if ten trials were completed for each target in both tasks. No other selection criteria have been applied. From the original population of 162 neurons, this procedure yielded 145 neurons for analysis (89 in monkey 1, M1, 56 in monkey 2, M2).

Single neuron activity was recorded and then quantified into spike counts calculated in 100ms bins that were then used to build up features population vectors to train the MLE and Naïve Bayes (NB) decoders. Thus a single features vector included, for a given time bin, spike counts calculated for each element (neuron) of the examined population, that is 89 elements for monkey 1 and 56 for monkey 2. Features space was obtained concatenating horizontally all 10 trials by 9 possible positions (90 feature vectors). Note that neurons were recorded one at time, therefore feature vectors describe the activity of a pseudo-population (2.3.1).

1
2
3 257 We were interested in studying to what extent signals extracted from V6A could support cognitive neuro
4
5 258 prosthetics. Unlike the traditional approach where the trajectory of movement is decoded, here we used a
6
7
8 259 combinations of MLE and NB decoders to decode: a) target location, b) the intention to perform a reach or a
9
10 260 non-spatial motor response and c) the different phases that follow one another for the realization of the
11
12 261 movement, free, delay and movement.

13
14 262
15
16 263 *3.1 Target decoding.* The first property we decoded was target position in space. We have previously decoded
17
18 target position in categorical space (left/right, near/far) using a Bayesian classifier (42). Given that the space
19 264 is a continuous physical quantity, such method would have insufficient application in real life conditions. To
20
21 265 overcome this limitation, we employed here an MLE decoder which, starting from the x, y coordinates of
22
23 266 target position in space (x, y for direction and depth axis, respectively) and the corresponding spike counts,
24
25 267 fitted a polynomial regression surface for each neuron. Using Bayes' rule we calculated continuous maps
26
27 268 which describe the probability of target's x, y location given a spike count. Combining maps across neurons
28
29 269 we obtained the most likely target position given the population spike counts vector.

30
31
32 270
33
34 271
35
36 272 Figure 3 reports the results of this analysis performed on a time interval that spanned from 500ms before,
37
38 273 till the movement onset for M1 and M2 populations. Averaged decoded positions (black dots) were typically
39
40 274 very close to the real position of targets (green crosses). Estimated positions using signals from M1
41
42 275 population ($n=89$) yielded good accuracy and precision: we calculated an overall mean constant error (over
43
44 276 100 cross validations and 9 positions) of 1.1 cm (S.D. 1.1) and a mean dispersion of 1.4 cm (Fig.3 left, S.D.
45
46 277 1.2). For M2 population, we found similar results with a mean constant error of 0.9 cm (SD 0.6) and a mean
47
48 278 dispersion of 2.3 cm (Fig.3 right, SD 2.1). Besides a lower accuracy for M2 monkey probably due to a smaller
49
50 279 neural population, results were very comparable between the two monkeys. Similar results were obtained
51
52 280 pooling together neurons from M1 and M2 (compare M1 results with Fig.4 where M1 + M2 population was
53
54 281 used) with an even higher precision and accuracy, 1.1cm, SD 0.7, and 1.1cm, SD 0.8, respectively. The analyses
55
56 282 presented below were obtained by pooling together data from M1 and M2.

60

283

284

285

286

287

288

289

290

291

292

293

294

295

296

297

298

299

300

301

302

303

304

305

306

307

308

309

First, we analyzed three distinct 300-ms intervals in each task (Fig. 1D). The first interval, termed ‘early delay’, extended from the beginning of target fixation till 300 ms after it. The second interval, ‘late delay’, included the last 300 ms before the ‘Go’ cue. While in ‘early delay’ visuospatial signals related to the newly fixated target were expected to be dominant, in the ‘late delay’ we assumed that activity would also be influenced by the preparation of the upcoming movement. The third interval we analyzed started at the ‘GO’ cue and lasted for 300 ms, thus encompassing monkey’s reaction time, which is variable between trials (285 ms SD 44 ms), and part of movement (409 ms SD 99 ms from the release of the home button to the touch of the target). By examining these three intervals we examined whether decoding accuracy of target’s location changes across distinct task stages.

Overall results of Figure 4 show a high decoding performance in all three intervals. Decoding accuracy increased moving toward the movement onset, with distances (ellipses size) between predicted and real target position progressively decreasing throughout the task. No remarkable differences were noticeable between the fix-reach and fix-lift tasks (Mann-Whitney test, $p > 0.05$).

While using wide time intervals (i.e. 300 ms) for the analysis reduces noise increasing overall decoding performance, it provides less information about the dynamics of neural coding. To resolve this issue, we performed the same decoding analysis using a 100-ms window that moved in steps of 20 ms. A full 100-fold cross-validation was performed, R^2 values were plotted as function of time (Fig. 5). Blue and red solid lines of Figure 5 refer to R^2 values for cross-validated models of fix-reach and fix-lift tasks, respectively. Decoding accuracy started to increase as soon as the target was presented (Fig.1, LED ON), was stable during delay and movement and then decreased at the end of each task. This performance was used as reference for the generalization analysis. With this analysis we investigated how much the task-specific movements (reach vs hand lift) affected the population activity. Generalization typically works well in case of similar pattern of neural activity, whereas poor results are obtained when neural codes differ. The generalization analysis was implemented by training the MLE decoding algorithm on one task and testing it on the other task, with results

plotted as dashed lines in Figure 5. As shown, the generalization performance during the delay epoch was comparable with decoding performed within the same task (solid lines), suggesting that activity during delay reflected mostly an abstract encoding of movement preparation and/or cue anticipation shared between the two tasks. Differently, after GO signal the generalization performance dropped abruptly. This finding most likely reflects the different motor response (reach vs. hand lift).

3.2. Task decoding. The generalization analysis reported in Figure 5 showed that the patterns of population activity in the two tasks were similar during the delay period and then they diverged immediately before and during the movement. The similarity during the delay makes questionable whether it is feasible to extract task-specific information from the activity before the movement execution. This information would be useful for a prosthesis about the real intention of the subject. To maximize the differences in neuronal activity linked to the specific movement plans of the two tasks and to allow a decoder to better discriminate between them, we performed another analysis. We used the residuals from regressions fits performed for the MLE decoding described above as feature to train a Naïve Bayes classifier. Residuals describe how much the observed data (spike counts) deviated from the model; in this case, polynomial fit was calculated pooling together the fix-reach and fix-lift datasets, thus plausibly the model was halfway between the real data of fix-reach and fix-lift, making the residuals suitable to describe the differences. As shown in Figure 6 the Naïve Bayes decoder correctly assigned, to fixate-to-reach or fixate-to-lift, residuals coming from the polynomial model. Recognition rates were above 90% before and after the GO signal, thus confirming the feasibility of extracting the task-specific motor plan well before movement onset.

3.3. State decoding. To develop neural prosthetics as autonomous as possible, the algorithm would have to determine when the subject intend to start the action. Decoding of neural states has been pursued as trigger for neuroprosthetic control (17,34). Yet identifying the exact temporal sequence of neural states can help to understand how similar neural activation patterns are reused in different tasks, and how these latent states gradually evolve towards movement execution (43). PPC seems to be the ideal region to extract information

regarding task phases, as PPC neurons often exhibit activity modulation according to the task phase (24,29,44,45). To examine this aspect, we trained a Naive Bayes classifier to recognize the correct task phase between FREE, DELAY and MOV epochs given the spike counts in these epochs. We found that the high probabilities of a certain state matched the behavioral epoch that was source of spike counts. Accordingly, it was possible to identify the correct task state giving spike counts from a random 100 ms bin (Fig. 7A, top row) both for fix-reach and fix-lift. Applying the generalization approach (Fig. 7A, bottom row) yielded accurate epoch recognition during FREE and DELAY (i.e. the fix-reach and fix-lift codes are very similar). As expected, MOVEMENT epoch is not recognized in the context of generalization because of the very different nature of movement type between the tasks (reaching vs hand lift). Accuracy score for single classes (epochs) reported in confusion matrices (Fig.7B) are consistent with state probabilities of Fig.7A: codes are very similar during free and delay epoch, but not during MOV. For the MOV epoch, in particular where the decoder was trained during the fix-reach and tested during the fix-lift task, the classifier yielded a rather unexpected result. In fact, state probabilities were unbalanced towards being in the state delay (see green line in the corresponding box of Fig.7A), this lead to a bias in the confusion matrix where a 33% chance level was expected (here 83% of MOV bins were attributed to the delay epoch). The result indicates that during the movement epoch of the fix-lift task visuospatial information that is present also in fix-reach task is preserved. On the contrary, visuospatial signals in fix-lift task were not strong enough to support decoding generalization in the fix-reach task. In other words, while in the case of the fix-reach task the information about the spatial position of the target remained relevant during MOV, this was not the case for the corresponding interval of the fix-lift task where the simple release of the button did not require spatial information.

4. Discussion

We examined whether we could decode from the population activity of PPC area V6A information regarding the target position, the required movement type and the time interval along the task progress at the same time. We trained a MLE algorithm to yield a metric estimation of the target positions. Then we used a combination of MLE and a NB classifier to obtain a classification of task type. Finally, we demonstrated that,

1
2
3 361 supplying the algorithm with spike counts from small time intervals of the trial, these were attributed
4
5 362 correctly to the corresponding free, delay or movement epoch.
6
7 363 Taken together, these results indicate that neurons in V6A encode, in the same population, several types of
8
9
10 364 information such as spatial position, intention for a specific motor response and progress of the task. This
11
12 365 finding supports the idea that neurons are not simply tuned to a single feature, but they encode several task-
13
14 366 relevant variables in the same time. Decoding of multiple parameters from the same area could be
15
16 367 advantageous for BCI applications in terms of implant invasiveness and accuracy of the reconstructed
17
18 368 information.
19
20
21 369
22
23 370
24
25 371

27
28 372 *4.1 Decoding of visuospatial, movement planning and motor signals.*
29

30 373
31
32 374 Monkeys performed both tasks while always looking at the targets, so our task cannot discriminate whether
33
34 375 we are solely decoding gaze position or attentional/visuospatial signals useful to guide the motor response.
35
36 376 In a previous work where we dissociated gaze from target, the decoding of target position was still possible,
37
38 377 though less accurate (42). This suggested that V6A neurons carry both attentional and gaze signals. Signals
39
40 378 related to gaze position and visuospatial attention have been shown to be useful for decoding and
41
42 379 neuroprosthetic purposes (46–48). Thus, although in the present case it was not possible to separate the two
43
44 380 components, this is not a limitation for the proposed method, since often the spatial attention matches the
45
46 381 gaze position in naturalistic conditions.
47
48 382 Single cell analysis over the population used here showed that about 44% of cells were influenced by both
49
50 383 target location and task type. Another fraction of cells (25%) were tuned by target location, but not task type,
51
52 384 while a smaller number (17%) encoded task type only (33). Given the tight relationship between the tuning
53
54 385 of a neural population to a given parameter and the decoding accuracy of that parameter using population
55
56 386 activity(42,49–51), it should be taken for granted that each of the homogeneous sub-populations mentioned
57
58
59
60

above would excel in decoding the variable(s) that is tuned for. For example, the sub-population of cells sensitive only to the type of task (i.e. their firing rate does not significantly change between different spatial position), will not contribute to the spatial position decoding of the target, which would rely on signals from the other two subpopulations. At this regard, the reliable decoding of target position from population signals in both tasks (Fig.5), is in line with the high incidence (44% + 25%) of neurons sensitive to target location as reported in Breveglieri et al.(32) and was also confirmed by the generalization analysis. Our decoding analyses put together these subpopulations in order to extract information from the whole population activity and thus achieve the best decoding performance.

Generalization of decoders between tasks can help to examine the nature of encoded information. Different authors used a generalization approach to test stationarity of temporal code within a neural population (51–53), or to compare population activation patterns between different, but related tasks (43). Similarly, we wanted to compare codes employed for tasks that shared initial stages, but differed in the subsequent motor response and its related planning. After the GO signal, the neural population activity changed to encode the upcoming movement, so the decoder's generalization performance dropped rather abruptly.

Slightly before the Go signal, the generalization performance was still high, thus suggesting that planning activity was similar between the two tasks. This finding, though surprising, might be attributed to the presence of a default reach plan/intention also when no reach is executed, as some evidence suggests (54,55). However, given that the two tasks were performed in separate blocks, the animal was always aware whether it was required to perform a reach movement, or simply lift its hand. Furthermore, given that a simple hand lift was enough to obtain the reward, we would expect that monkey's intention and commitment to perform a reach was significantly attenuated in the fixation-to-lift task. In line with this view, Breveglieri et al. (33) found that the majority of V6A cells show different activity between these two tasks. Whether these neurons were still encoding a default or uncompleted reach plan cannot be answered directly in the present study. Nevertheless, we could still discriminate task type (Fig.6) despite the fact that the codes were very similar during the delay (code generalization of Fig. 5). Such a result would not have been achieved if the neural codes in the two tasks were the same. The high levels of generalization obtained in the period

before the movement could be attributed to the strong visuospatial signals in V6A that, being invariant between tasks, masked the task-specific signals related to movement planning and preparation. Our decoding method was based on fitting residuals. Residuals represent the distance between actual spike counts and regression surfaces: thinking at these surfaces as a midline between fixate-to-reach and fixate-to-lift condition (because of fitting of dispersed data), shifts from this midline are still informative about the task type. A point of strength of this analysis is the type of feature we used in the classifier. The model was computed pooling together data from different target positions; this ensures that the present method works independently from position constraints. The possibility to discriminate in advance if the subject will execute the reach movement or just lift the hand, could be potentially useful for neuroprosthetic purposes. In case where a Go signal is spatially dissociated from the target of the action (e.g. clicking a computer mouse while looking at the screen), decoded information may allow to select the appropriate action: to prepare for moving or to withhold the robotic limb. In our case the decoding is limited to distinguish two scenarios, but the system could be trained to recognize different tasks and act accordingly.

4.2 Metric estimation of target position from PPC.

In a previous work we used a Bayesian classifier from PPC activity to discriminate between the nine target positions on the same panel used here (42). This method yielded very high target recognition rates and a small neuronal population was sufficient to obtain very good results (about 10-20 neurons). The present method enables a metric estimation of target positions at the cost of a larger number of neurons required to give an accurate prediction. 56 neurons were found to be barely enough (see very high dispersion in M2 case) to get a good decoding accuracy, whereas ~90 neurons (see M1 case) were fairly enough. Given that simple (second-order) polynomials were used to model single neuron tuning, our results suggest that good performance could also be observed for intermediate target positions never seen by the decoder. This is a desirable characteristic for a fully implemented neural decoder.

439

4.3 Encoding of task progress.

Thus, V6A signals were adequate to obtain a metric estimation of target, both in the fix-reach and fix-lift task, and to decode the intended action. In addition, we provided evidence that a time interval of 100 ms, putting together contributions of a population of V6A neurons, was sufficient to decode reliably the corresponding phase in the task progress (Fig.7A-B). Although much effort has been put into decoding intended reaching goals (2,16,56), deciphering the intended action onset is equally important (17,34,57). Different task phases have been typically correlated to different neural states, proceeding through the tasks entail moving through neural states. So, in our fix-reach task we expected at least three neural states: a resting state (no task engagement), a waiting time where the animal waited the go signal and finally the actual reaching movement. A similar task was studied in premotor areas (34). They used a hidden Markov model (HMM) to detect baseline, preparation and execution states. In addition, they implemented an extended model to decode multiple states, one for each reaching goal. In another study a four states (additional holding state) HMM was used to detect hidden neural states and so to develop a task independent decoder (58). Here we used a simpler, but equally informative, Bayesian decoder to obtain posterior probabilities of free, delay and movement states. Our results demonstrate that also signals from V6A are adequate to detect the switch from pre-movement to movement neural state that might be useful to trigger neural prosthesis movement.

456

457

458

459

460

461

462

463

464

465

466

467

468

469

470

471

472

473

474

475

476

477

478

479

480

481

482

483

484

485

486

487

488

489

490

491

492

493

494

495

496

497

498

499

500

501

502

503

504

505

506

507

508

509

510

511

512

513

514

515

516

517

518

519

520

521

522

523

524

525

526

527

528

529

530

531

532

533

534

535

536

537

538

539

540

541

542

543

544

545

546

547

548

549

550

551

552

553

554

555

556

557

558

559

560

561

562

563

564

565

566

567

568

569

570

571

572

573

574

575

576

577

578

579

580

581

582

583

584

585

586

587

588

589

590

591

592

593

594

595

596

597

598

599

600

601

602

603

604

605

606

607

608

609

610

611

612

613

614

615

616

617

618

619

620

621

622

623

624

625

626

627

628

629

630

631

632

633

634

635

636

637

638

639

640

641

642

643

644

645

646

647

648

649

650

651

652

653

654

655

656

657

658

659

660

661

662

663

664

665

666

667

668

669

670

671

672

673

674

675

676

677

678

679

680

681

682

683

684

685

686

687

688

689

690

691

692

693

694

695

696

697

698

699

700

701

702

703

704

705

706

707

708

709

710

711

712

713

714

715

716

717

718

719

720

721

722

723

724

725

726

727

728

729

730

731

732

733

734

735

736

737

738

739

740

741

742

743

744

745

746

747

748

749

750

751

752

753

754

755

756

757

758

759

760

761

762

763

764

765

766

767

768

769

770

771

772

773

774

775

776

777

778

779

780

781

782

783

784

785

786

787

788

789

790

791

792

793

794

795

796

797

798

799

800

801

802

803

804

805

806

807

808

809

810

811

812

813

814

815

816

817

818

819

820

821

822

823

824

825

826

applications, yet few works tried to perform population decoding of both spatial and non-spatial PPC signals and explore the potential from a neuroprosthetic perspective. In Hauschild et al.(14), monkey brain activity controlled a cursor in a 3D environment, but the cognitive information that can be decoded from PPC to improve the decoder was not considered. Similarly another study by Shenoy and colleagues (17) decoded the information about task stage, either free, plan or movement, but they did not attempt to generalize the decoder over other tasks.

Recent studies have demonstrated that neurons in parietal (24,63–68) and frontal (69,70) areas have mixed selectivity: individual neurons are modulated by multiple task parameters. Rather than having specialized networks for specific behaviors, mixed selectivity is considered to offer a significant computational advantage by encoding multiple feature information over a single neural network (69,71,72). In everyday life, we often look at objects that we are going to reach and grasp, but we also look and attend to stimuli in one location and perform a motor response in another location. Here we provide evidence that both action plans that involve different sensory-to-motor transformations can be decoded from the same neural population in V6A and this finding is relevant also as fundamental knowledge.

4.5 Future application in human.

Functional MRI studies proposed a putative human homologue of area V6A (35), which approximately corresponds to the anterior part of the superior parieto-occipital cortex (SPOC) (12). SPOC shows enhanced visual activation to objects presented within the peripersonal space, even when the potential action is not actually executed (73). Decoding of pre-movement activity of SPOC with fMRI pattern analysis allowed reliable classification of specific actions that were subsequently performed, with a clear distinction between reaching and grasping movements (19). Although fMRI technique does not allow to study mixed selectivity due to poor spatial resolution, analogies between monkey and putative human V6A (35,74) give hope to translate findings from monkey to human.

5. Conclusions

In conclusion, these results show that V6A signals can be used to reliably decode visuospatial properties, information about the type of intended movement (spatial, goal-directed reach, or non-spatial button release), and task progression. Recently, V6A signals were used to decode up to 5 grip types during a grasping task and 9 different goal locations during reach (41,42). Previous and present results support prostheses that extract the target of a movement and respond as the intention to move is formed. Furthermore, present findings show that conditional motor responses like when a visual cue instructs a movement somewhere else in space could be also decoded and subsequently used to control a prosthesis. Having multiple information coded in a single area is advantageous for neuroprosthetics, allowing a single electrode array to decode multiple action scenarios.

Funding

This work was supported by European Union (H2020-MSCA-734227 – PLATYPUS), by Ministero dell'Università e della Ricerca (Italy, PRIN2017-2017KZNZLN), by Fondazione Cassa di Risparmio in Bologna, Bando Ricerca 2018/0373, by National Health and Medical Research Council (Australia, NHMRC APP1083898, NHMRC APP1082144).

Acknowledgements

We thank Drs. Federica Bertozzi and Giulia Dal Bo' for help in the recordings, Massimo Verdosci and Francesco Campisi for technical assistance.

References

- Hochberg LR, Bacher D, Jarosiewicz B, Masse NY, Simeral JD, Vogel J, et al. Reach and grasp by people with tetraplegia using a neurally controlled robotic arm. *Nature*. 2012;485(7398):372–5.
- Aflalo T, Kellis S, Klaes C, Lee B, Shi Y, Pejsa K, et al. Neurophysiology. Decoding motor imagery from the posterior parietal cortex of a tetraplegic human. *Science*. 2015 May 22;348(6237):906–10.
- Collinger JL, Wodlinger B, Downey JE, Wang W, Tyler-Kabara EC, Weber DJ, et al. High-performance neuroprosthetic control by an individual with tetraplegia. *Lancet*. 2013 Feb;381(9866):557–64.
- Velliste M, Perel S, Spalding M, Whitford A, Schwartz A. Cortical control of a robotic arm for self-feeding. *Nature*. 2008;453(June):1098–101.
- Carmena JM, Lebedev MA, Crist RE, O'Doherty JE, Santucci DM, Dimitrov DF, et al. Learning to control a brain-machine interface for reaching and grasping by primates. *PLoS Biol*. 2003;1(2):E42.
- Wessberg J, Stambaugh CR, Kralik JD, Beck PD, Laubach M, Chapin JK, et al. Real-time prediction of hand trajectory by ensembles of cortical neurons in primates. *Nature*. 2000;408(6810):361–5.
- Mountcastle VB, Lynch JC, Georgopoulos A, Sakata H, Acuna C. Posterior parietal association cortex of the monkey: command functions for operations within extrapersonal space. *J Neurophysiol*. 1975 Jul 1;38(4):871–908.
- Andersen RA, Snyder LH, Bradley DC, Xing J. MULTIMODAL REPRESENTATION OF SPACE IN THE

- 1
- 2
- 3 528 POSTERIOR PARIETAL CORTEX AND ITS USE IN PLANNING MOVEMENTS. *Annu Rev Neurosci.* 1997;
- 4 529 9. Andersen RA, Burdick JW, Musallam S, Pesaran B, Cham JG. Cognitive neural prosthetics. Vol. 8,
- 5 530 Trends in Cognitive Sciences. 2004. p. 486–93.
- 6 531 10. Kalaska JF, Scott SH, Cisek P, Sergio LE. Cortical control of reaching movements. *Curr Opin Neurobiol.*
- 7 532 1997 Dec;7(6):849–59.
- 8 533 11. Culham JC, Cavina-Pratesi C, Singhal A. The role of parietal cortex in visuomotor control: What have
- 9 534 we learned from neuroimaging? *Neuropsychologia.* 2006 Jan;44(13):2668–84.
- 10 535 12. Gallivan JP, Culham JC. Neural coding within human brain areas involved in actions. *Curr Opin*
- 11 536 *Neurobiol.* 2015 Aug;33:141–9.
- 12 537 13. Gallivan JP, Goodale MA. The dorsal “action” pathway. In: *Handbook of clinical neurology.* 2018. p.
- 13 538 449–66.
- 14 539 14. Hauschild M, Mulliken GH, Fineman I, Loeb GE, Andersen RA. Cognitive signals for brain-machine
- 15 540 interfaces in posterior parietal cortex include continuous 3D trajectory commands. *Proc Natl Acad*
- 16 541 *Sci U S A.* 2012 Oct;109(42):17075–80.
- 17 542 15. Mulliken GH, Musallam S, Andersen RA. Decoding trajectories from posterior parietal cortex
- 18 543 ensembles. *J Neurosci.* 2008;28(48):12913–26.
- 19 544 16. Musallam S, Corneil BD, Greger B, Scherberger H, Andersen R. Cognitive control signals for neural
- 20 545 prosthetics. *Science.* 2004;305(5681):258–62.
- 21 546 17. Shenoy K V., Kureshi SA, Pesaran B, Buneo CA, Andersen RA, Meeker D, et al. Neural prosthetic
- 22 547 control signals from plan activity. *Neuroreport.* 2003 Mar 24;14(4):591–6.
- 23 548 18. Gertz H, Lingnau A, Fiehler K. Decoding Movement Goals from the Fronto-Parietal Reach Network.
- 24 549 *Front Hum Neurosci.* 2017 Feb 24;11.
- 25 550 19. Gallivan JP, McLean DA, Valyear KF, Pettypiece CE, Culham JC. Decoding action intentions from
- 26 551 preparatory brain activity in human parieto-frontal networks. *J Neurosci.* 2011 Jun 29;31(26):9599–
- 27 552 610.
- 28 553 20. Andersen RA, Cui H. Intention, Action Planning, and Decision Making in Parietal-Frontal Circuits.
- 29 554 *Neuron.* 2009 Sep;63(5):568–83.
- 30 555 21. Hadjidimitrakis K, Bakola S, Wong YT, Hagan MA. Mixed Spatial and Movement Representations in
- 31 556 the Primate Posterior Parietal Cortex. *Front Neural Circuits.* 2019 Mar 11;13:15.
- 32 557 22. Galletti C, Fattori P, Kutz DF, Gamberini M. Brain location and visual topography of cortical area V6A
- 33 558 in the macaque monkey. *Eur J Neurosci.* 1999 Feb;11(2):575–82.
- 34 559 23. Galletti C, Kutz DF, Gamberini M, Breveglieri R, Fattori P. Role of the medial parieto-occipital cortex
- 35 560 in the control of reaching and grasping movements. In: *Experimental brain research.* 2003. p. 158–
- 36 561 70.
- 37 562 24. Hadjidimitrakis K, Bertozzi F, Breveglieri R, Bosco A, Galletti C, Fattori P. Common neural substrate
- 38 563 for processing depth and direction signals for reaching in the monkey medial posterior parietal
- 39 564 cortex. *Cereb Cortex.* 2014;24(6):1645–57.
- 40 565 25. Fattori P, Raos V, Breveglieri R, Bosco A, Marzocchi N, Galletti C. The dorsomedial pathway is not
- 41 566 just for reaching: grasping neurons in the medial parieto-occipital cortex of the macaque monkey. *J*
- 42 567 *Neurosci.* 2010;30(1):342–9.
- 43 568 26. Fattori P, Breveglieri R, Bosco A, Gamberini M, Galletti C. Vision for Prehension in the Medial Parietal
- 44 569 Cortex. *Cereb Cortex.* 2017 Dec 1;27(2):1149–63.
- 45 570 27. Hadjidimitrakis K, Breveglieri R, Bosco A, Fattori P. Three-dimensional eye position signals shape
- 46 571 both peripersonal space and arm movement activity in the medial posterior parietal cortex. *Front*
- 47 572 *Integr Neurosci.* 2012;6:37.
- 48 573 28. Fattori P, Gamberini M, Kutz DF, Galletti C. “Arm-reaching” neurons in the parietal area V6A of the
- 49 574 macaque monkey. *Eur J Neurosci.* 2001 Jun;13(12):2309–13.
- 50 575 29. Fattori P, Kutz DF, Breveglieri R, Marzocchi N, Galletti C. Spatial tuning of reaching activity in the
- 51 576 medial parieto-occipital cortex (area V6A) of macaque monkey. *Eur J Neurosci.* 2005 Aug;22(4):956–
- 52 577 72.
- 53 578 30. Hadjidimitrakis K, Breveglieri R, Placenti G, Bosco A, Sabatini SP, Fattori P. Fix your eyes in the space
- 54 579 you could reach: neurons in the macaque medial parietal cortex prefer gaze positions in

- peripersonal space. Gribble PL, editor. PLoS One. 2011 Aug 17;6(8):e23335.
31. Breveglieri R, Hadjidimitrakis K, Bosco A, Sabatini SP, Galletti C, Fattori P. Eye position encoding in three-dimensional space: integration of version and vergence signals in the medial posterior parietal cortex. *J Neurosci*. 2012 Jan 4;32(1):159–69.
 32. Hadjidimitrakis K, Ghodrati M, Breveglieri R, Rosa MGP, Fattori P. Neural coding of action in three dimensions: Task- and time-invariant reference frames for visuospatial and motor-related activity in parietal area V6A. *J Comp Neurol*. 2020;
 33. Breveglieri R, Galletti C, Dal Bò G, Hadjidimitrakis K, Fattori P. Multiple aspects of neural activity during reaching preparation in the medial posterior parietal area V6A. *J Cogn Neurosci*. 2014 Apr;26(4):878–95.
 34. Kemere C, Santhanam G, Yu BM, Afshar A, Ryu SI, Meng TH, et al. Detecting Neural-State Transitions Using Hidden Markov Models for Motor Cortical Prostheses. *J Neurophysiol*. 2008;100(4):2441–52.
 35. Pitzalis S, Sereno MI, Committeri G, Fattori P, Galati G, Tosoni A, et al. The human homologue of macaque area V6A. *Neuroimage*. 2013 Nov 15;82:517–30.
 36. Galletti C, Fattori P, Gamberini M, Kutz DF. The cortical visual area V6: brain location and visual topography. *Eur J Neurosci*. 1999 Nov;11(11):3922–36.
 37. Morris AP, Krekelberg B. A Stable Visual World in Primate Primary Visual Cortex. *Curr Biol*. 2019 May 6;29(9):1471–1480.e6.
 38. Morris AP, Bremmer F, Krekelberg B. Eye-position signals in the dorsal visual system are accurate and precise on short timescales. *J Neurosci*. 2013 Jul 24;33(30):12395–406.
 39. Morris AP, Kubischik M, Hoffmann K-P, Krekelberg B, Bremmer F. Dynamics of Eye-Position Signals in the Dorsal Visual System. *Curr Biol*. 2012 Feb 7;22(3):173–9.
 40. Morris AP, Bremmer F, Krekelberg B. The Dorsal Visual System Predicts Future and Remembers Past Eye Position. *Front Syst Neurosci*. 2016 Feb 24;10:9.
 41. Filippini M, Breveglieri R, Akhras MA, Bosco A, Chinellato E, Fattori P. Decoding Information for Grasping from the Macaque Dorsomedial Visual Stream. *J Neurosci*. 2017 Apr;37(16):4311–22.
 42. Filippini M, Breveglieri R, Hadjidimitrakis K, Bosco A, Fattori P. Prediction of Reach Goals in Depth and Direction from the Parietal Cortex. *Cell Rep*. 2018;23(3):725–32.
 43. Mazurek KA, Rouse AG, Schieber MH. Mirror Neuron Populations Represent Sequences of Behavioral Epochs During Both Execution and Observation. *J Neurosci*. 2018 May 2;38(18):4441–55.
 44. Cui H, Andersen RA. Posterior Parietal Cortex Encodes Autonomously Selected Motor Plans. *Neuron*. 2007;56(3):552–9.
 45. Stetson C, Andersen RA. Early planning activity in frontal and parietal cortex in a simplified task. *J Neurophysiol*. 2015 Jun;113(10):3915–22.
 46. Astrand E, Wardak C, Ben Hamed S. Selective visual attention to drive cognitive brain machine interfaces: from concepts to neurofeedback and rehabilitation applications. *Front Syst Neurosci*. 2014 Aug 12;8.
 47. Andersen RA, Hwang EJ, Mulliken GH. Cognitive neural prosthetics. *Annu Rev Psychol*. 2010 Jan;61:169–90, C1–3.
 48. Batista AP, Yu BM, Santhanam G, Ryu SI, Afshar A, Shenoy KV. Cortical Neural Prosthesis Performance Improves When Eye Position Is Monitored. *IEEE Trans Neural Syst Rehabil Eng*. 2008 Feb;16(1):24–31.
 49. Bremmer F, Kaminarz A, Klingenhoefer S, Churan J. Decoding target distance and saccade amplitude from population activity in the macaque lateral intraparietal area (LIP). *Front Integr Neurosci*. 2016;
 50. Lehmann SJ, Scherberger H. Reach and gaze representations in macaque parietal and premotor grasp areas. *J Neurosci*. 2013 Apr 17;33(16):7038–49.
 51. Astrand E, Ibos G, Duhamel J-R, Ben Hamed S. Differential Dynamics of Spatial Attention, Position, and Color Coding within the Parietofrontal Network. *J Neurosci*. 2015 Feb 18;35(7):3174–89.
 52. Crowe DA, Averbeck BB, Chafee M V. Rapid Sequences of Population Activity Patterns Dynamically Encode Task-Critical Spatial Information in Parietal Cortex. *J Neurosci*. 2010 Sep 1;30(35):11640–53.
 53. Meyers EM, Freedman DJ, Kreiman G, Miller EK, Poggio T. Dynamic Population Coding of Category Information in Inferior Temporal and Prefrontal Cortex. *J Neurophysiol*. 2008 Sep;100(3):1407–19.

- 1
- 2
- 3 632 54. Suminski AJ, Tkach DC, Hatsopoulos NG. Exploiting multiple sensory modalities in brain-machine
- 4 633 interfaces. *Neural Networks*. 2009 Nov;22(9):1224–34.
- 5 634 55. Bremner LR, Andersen RA. Temporal Analysis of Reference Frames in Parietal Cortex Area 5d during
- 6 635 Reach Planning. *J Neurosci*. 2014 Apr 9;34(15):5273–84.
- 7 636 56. Shanechi MM, Williams ZM, Wornell GW, Hu RC, Powers M, Brown EN. A Real-Time Brain-Machine
- 8 637 Interface Combining Motor Target and Trajectory Intent Using an Optimal Feedback Control Design.
- 9 638 Zhan W, editor. *PLoS One*. 2013 Apr 10;8(4):e59049.
- 10 639 57. Kao JC, Nuyujukian P, Ryu SI, Shenoy K V. A High-Performance Neural Prosthesis Incorporating
- 11 640 Discrete State Selection with Hidden Markov Models. *IEEE Trans Biomed Eng*. 2017;
- 12 641 58. Sumsy SL, Schieber MH, Thakor N V., Sarma S V., Santaniello S. Decoding kinematics using task-
- 13 642 independent movement-phase-specific encoding models. *IEEE Trans Neural Syst Rehabil Eng*. 2017;
- 14 643 59. Andersen RA, Buneo CA. Intentional Maps in Posterior Parietal Cortex. *Annu Rev Neurosci*. 2002;
- 15 644 60. Snyder LH, Batista a P, Andersen R a. Coding of intention in the posterior parietal cortex. Vol. 386,
- 16 645 *Nature*. 1997. p. 167–70.
- 17 646 61. Bisley JW, Goldberg ME. Attention, Intention, and Priority in the Parietal Lobe. *Annu Rev Neurosci*.
- 18 647 2010 Jun;33(1):1–21.
- 19 648 62. Ibos G, Freedman DJ. Interaction between Spatial and Feature Attention in Posterior Parietal Cortex.
- 20 649 *Neuron*. 2016 Aug 17;91(4):931–43.
- 21 650 63. Rishel CA, Huang G, Freedman DJ. Independent Category and Spatial Encoding in Parietal Cortex.
- 22 651 *Neuron*. 2013 Mar;77(5):969–79.
- 23 652 64. Meister MLR, Hennig JA, Huk AC. Signal Multiplexing and Single-Neuron Computations in Lateral
- 24 653 Intraparietal Area During Decision-Making. *J Neurosci*. 2013;
- 25 654 65. Park IM, Meister MLR, Huk AC, Pillow JW. Encoding and decoding in parietal cortex during
- 26 655 sensorimotor decision-making. *Nat Neurosci*. 2014 Oct 31;17(10):1395–403.
- 27 656 66. Hadjidimitrakis K, Bertozzi F, Breveglieri R, Galletti C, Fattori P. Temporal stability of reference
- 28 657 frames in monkey area V6A during a reaching task in 3D space. *Brain Struct Funct*. 2017 May
- 29 658 1;222(4):1959–70.
- 30 659 67. Bosco A, Breveglieri R, Hadjidimitrakis K, Galletti C, Fattori P. Reference frames for reaching when
- 31 660 decoupling eye and target position in depth and direction. *Sci Rep*. 2016 Apr 15;6(1):21646.
- 32 661 68. Bosco A, Breveglieri R, Filippini M, Galletti C, Fattori P. Reduced neural representation of arm/hand
- 33 662 actions in the medial posterior parietal cortex. *Sci Rep*. 2019 Dec 30;9(1):936.
- 34 663 69. Rigotti M, Barak O, Warden MR, Wang X-J, Daw ND, Miller EK, et al. The importance of mixed
- 35 664 selectivity in complex cognitive tasks. *Nature*. 2013 May 19;497(7451):585–90.
- 36 665 70. Mante V, Sussillo D, Shenoy K V., Newsome WT. Context-dependent computation by recurrent
- 37 666 dynamics in prefrontal cortex. *Nature*. 2013 Nov 6;503(7474):78–84.
- 38 667 71. Fusi S, Miller EK, Rigotti M. Why neurons mix: high dimensionality for higher cognition. *Curr Opin*
- 39 668 *Neurobiol*. 2016 Apr;37:66–74.
- 40 669 72. Zhang CY, Aflalo T, Revechkis B, Rosario ER, Ouellette D, Pouratian N, et al. Partially Mixed Selectivity
- 41 670 in Human Posterior Parietal Association Cortex. *Neuron*. 2017;
- 42 671 73. Gallivan JP, McLean A, Culham JC. Neuroimaging reveals enhanced activation in a reach-selective
- 43 672 brain area for objects located within participants' typical hand workspaces. *Neuropsychologia*. 2011
- 44 673 Nov;49(13):3710–21.
- 45 674 74. Tosoni A, Pitzalis S, Committeri G, Fattori P, Galletti C, Galati G. Resting-state connectivity and
- 46 675 functional specialization in human medial parieto-occipital cortex. *Brain Struct Funct*. 2015
- 47 676 Nov;220(6):3307–21.
- 48 677
- 49 678
- 50
- 51
- 52
- 53
- 54
- 55
- 56
- 57
- 58
- 59
- 60

Figures:

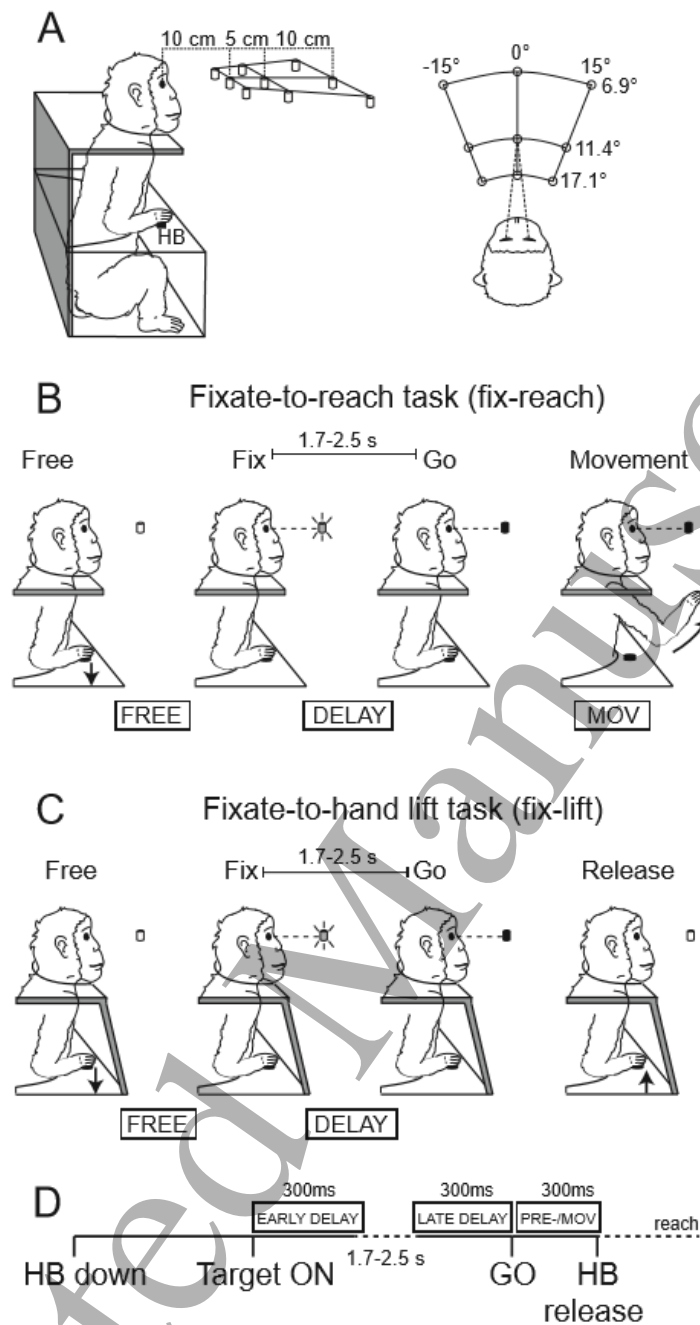


Figure 1. Experimental setup and schematic representation of the tasks. (A) Scheme of the setup used for the fix-reach and fix-lift tasks. Exact distances are indicated in the lateral (left) and top (right) views. Nine LEDs are used as targets, embedded in a panel located at eye level. HB = home button. (B, C) Time courses and behavioral epochs in the fix-reach (B) and fix-lift (C) tasks. The two tasks shared the first part, holding of home button, start of fixation, waiting for the GO signal. Then, in the fix-reach task the reaching movement is performed cued by the GO signal (target color changed from green to red), whereas in the fix-lift task the GO signal was the cue to lift the hand from the home button, and no reaching movement was performed. Black arrows indicate hand actions performed in the two tasks. (D) Schematic of the time intervals used in the analysis, with every interval lasting 300 ms. EARLY DELAY, from the start of the target fixation till 300 ms after it; LATE DELAY, the last 300 ms before the GO signal; PRE-/MOV, from the GO signal to 300 ms after it, this encompassed the reaction time plus the very first part of movement.

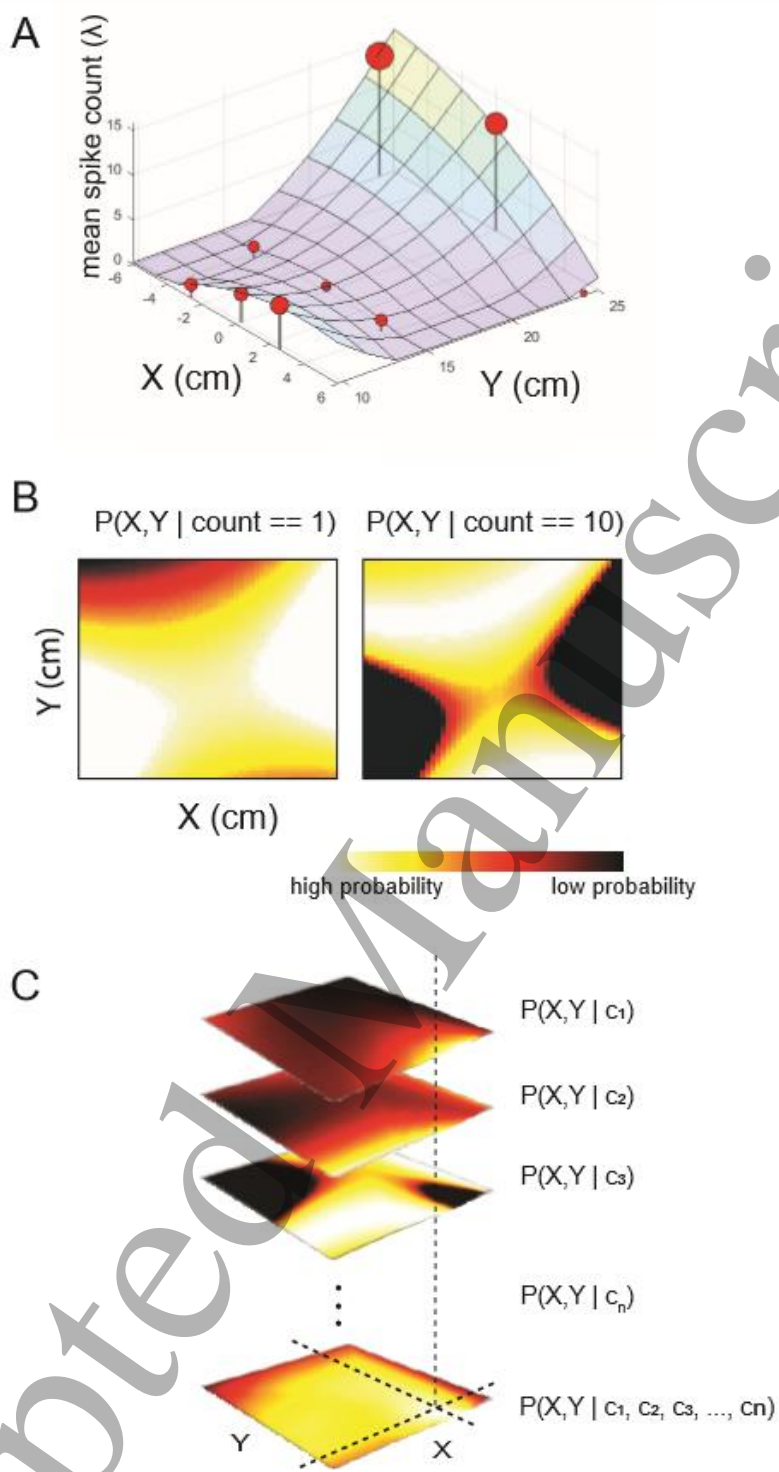


Figure 2. MLE decoder. (A) Activity of an exemplary V6A neuron and regression surface. In a first step a GLM was used to fit a regression surface over spike counts in the training set. Black vertical solid lines depict mean spike counts over the 9 panel positions with their standard deviation (red spheres). This neuron discharged for far positions, especially for the far-left position and was downregulated for intermediate positions. The regression surface was interpreted probabilistically, such that it specified the conditional probability of spike count given x,y target positions ($p(\text{count} | X,Y)$), assuming spike counts were Poisson-distributed. Using Bayes' rule, this could be converted to the probability of all target positions, X,Y , given a spike count ($p(X,Y | \text{count})$) in the test set. In (B) left, the probability map of neuron (A) given a low spike count (high probability in intermediate area) and (B) right, the probability maps given a high spike count (high probability for far and near area). (C) Given a vector of spike counts (c) for all neurons in a sample, (c_1, c_2, \dots, c_n), and corresponding probability maps, a population probability map was obtained by

summing the (log) probabilities. As the final step, the target position associated with the maximum a posteriori (MAP) log-likelihood (i.e., the MAP estimate) in $\log p(X,Y | \text{CountPopulation})$ was selected as the point estimate.

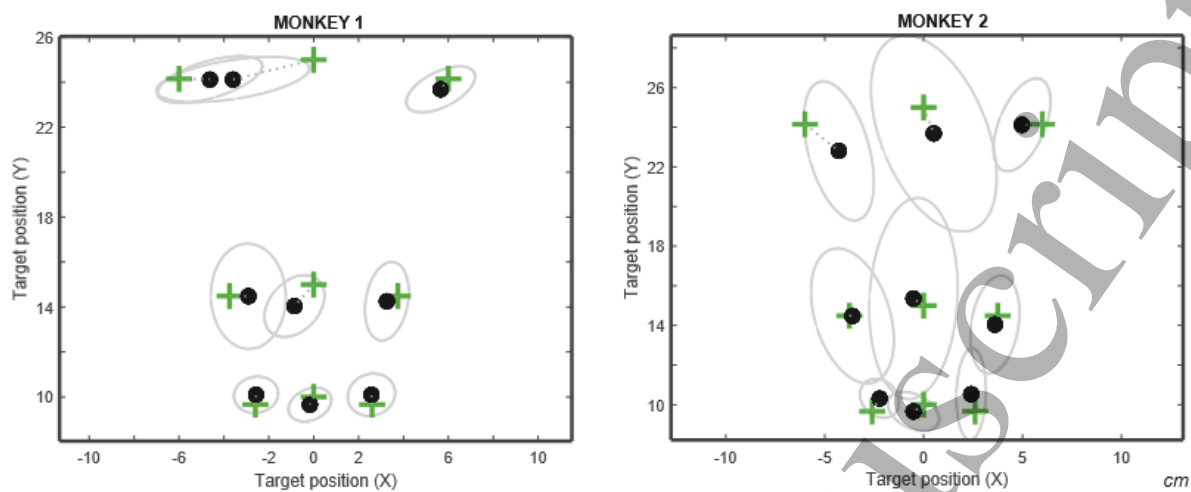


Figure 3. Metric estimation of target positions. The array of the 9 targets is illustrated in a two-dimensional view from above, green crosses show the real position of each targets, black dots are target estimated positions with their error distribution (light grey ellipses). Distances are reported in cartesian x,y (cm) coordinates, with x being the distance from the monkey's midsagittal level and y being the distance from the frontal eye level. Left panel, monkey 1 (89 neurons), right panel monkey 2 (56 neurons). Time analyzed was an interval of 500 ms before movement onset.

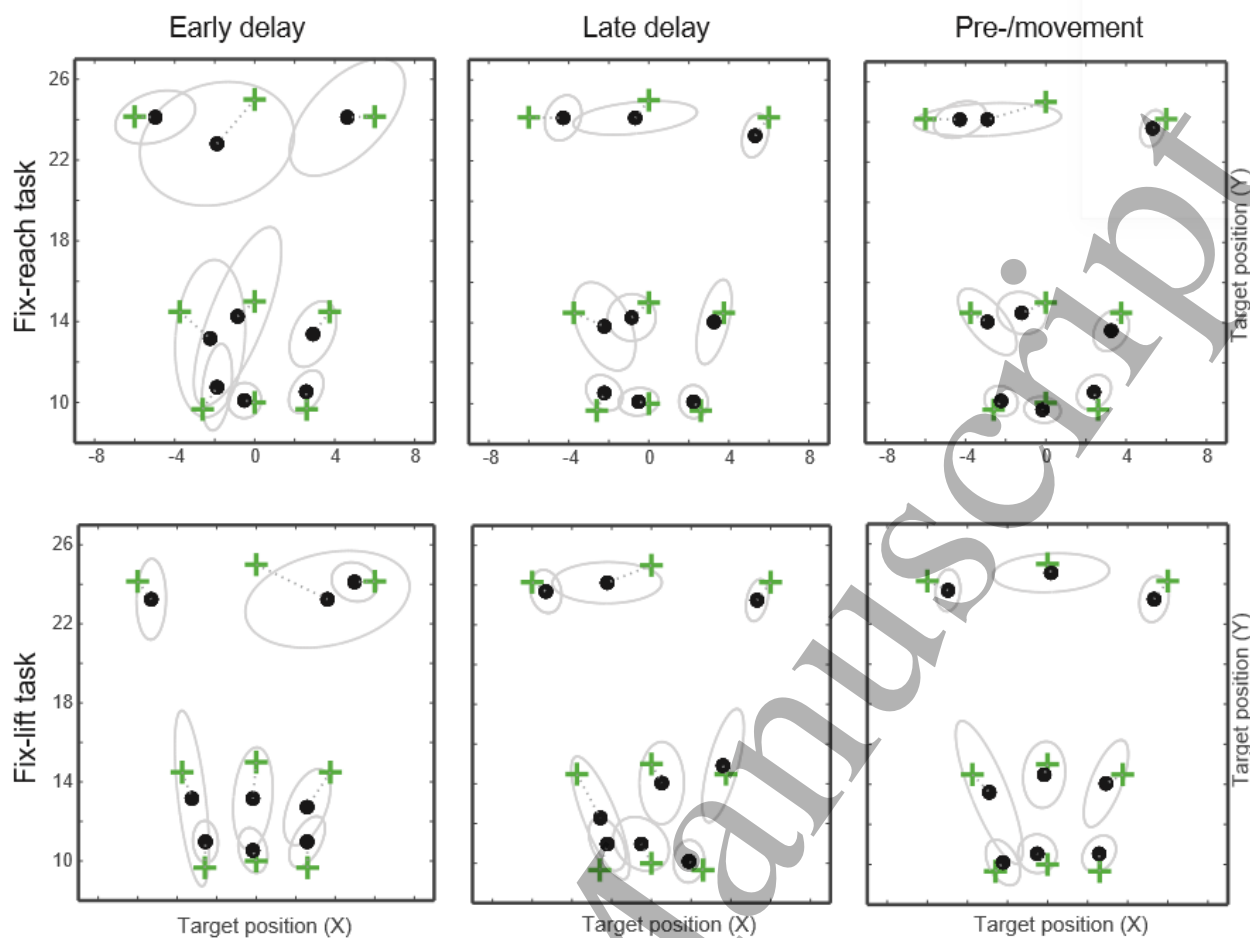


Figure 4. Metric estimation of targets position for different time intervals and tasks. Analysis was performed extracting spike counts from 100 ms time intervals and pooled together in 300 ms time windows corresponding to EARLY DELAY, LATE DELAY and PRE-/MOV epochs. These time intervals were analyzed for fix-reach task (top) where target position signals were transformed into arm action, and fix-lift task where no reaching movement was required (bottom). Neural population used in the analysis included both neurons from monkey 1 and monkey 2. Other conventions same as Figure 3.

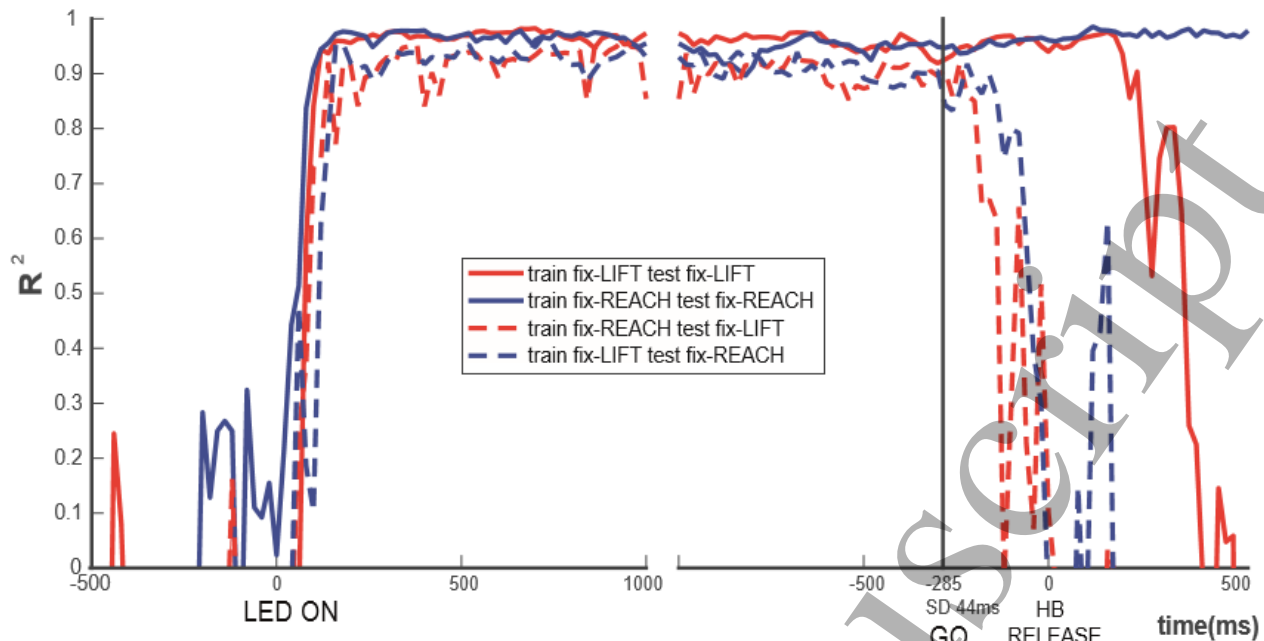


Figure 5. Decoding time course. R^2 values are reported for each of 100ms time intervals analyzed. The time window slid over the trial time with a 20ms step. Cross validated results are reported for fix-lift (solid red line) and fix-reach (solid blue line) tasks. A code generalization approach was used to obtain target estimations using the decoder trained with the opposite task dataset, that is, the algorithm was trained on fix-lift task and the code was generalized to decode fix-reach neural activity (blue dashed line), as opposed to training on fix-reach and estimation on fix-lift task (red dashed line). The plot required a double alignment (target LED ON and HB RELEASE, i.e. movement onset), as delay was randomized between trials. During the initial fixation and delay epochs across-task decoder performance was comparable to its within-task performance. This suggests that visuospatial and motor preparation codes were similar during the delay period. The two codes diverged shortly after the cue to execute the required motor response (reach/hand lift).

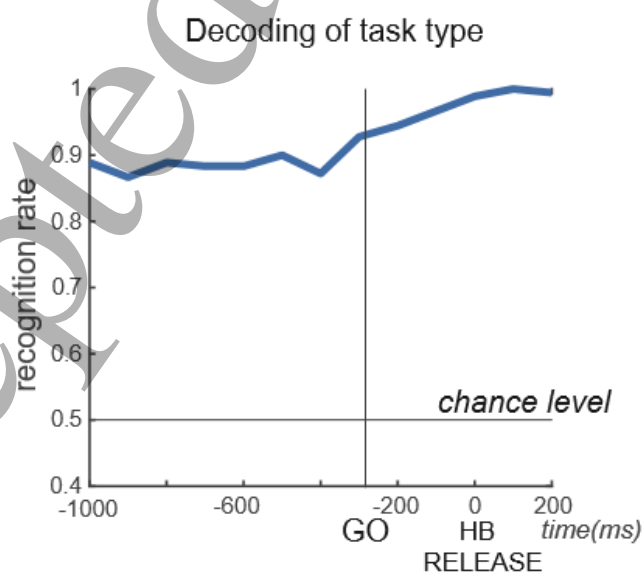


Figure 6. Decoding of task type. Binary classification of task type obtained feeding a naïve Bayes classifier with residuals from polynomial fits. Data from different targets were pooled together. A 50 folds' cross

1

2

3 743 validation was used. Residuals were good predictors for task type discriminations as evidenced by the

4 744 recognition rate being always well above chance levels.

5 745

6 746

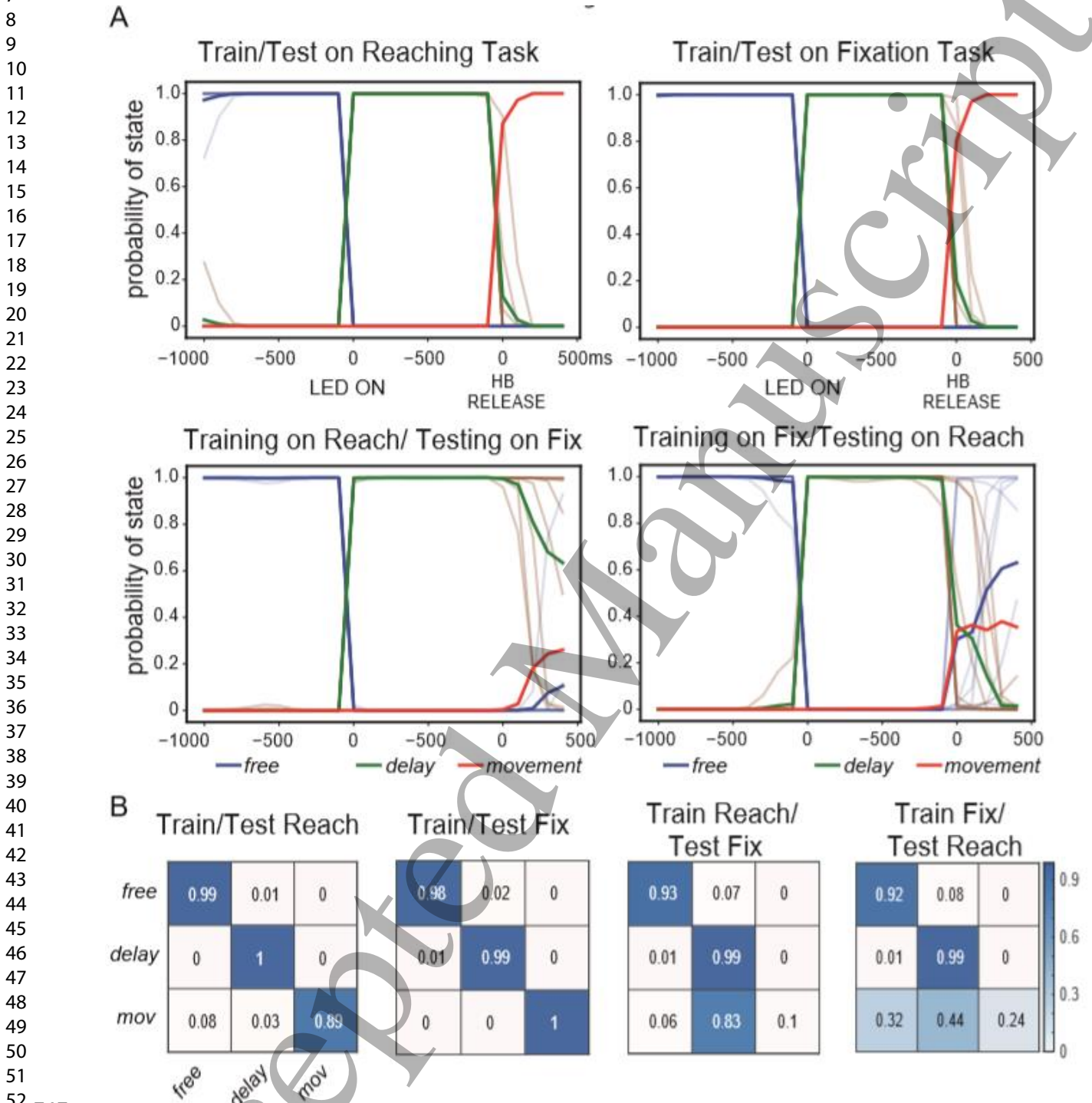


Figure 7. Decoding of task state. Spike counts were used as predictor of different task phases, free, delay or movement epochs. (A) Probability of each state, blue, green or red, respectively free, delay and movement states, were plotted over the time. Solid bold lines correspond to averages calculated over single trial probabilities (light lines). Due to different durations of delay between trials, two separate time intervals were artificially merged: 1 second before target led on (free epoch) and from -1.5s to 0.5s centered on movement onset. On the top row within-task decoding for reaching (left) and fixation (right) task are

shown, “leave one out” cross validation was used. Bottom row reports task generalization performance, i.e. training on fix-reach and testing on fix-lift task (left), and vice versa (right). During free and delay epochs the decoder can generalize across tasks; this gives an accurate epoch recognition, whereas movement epoch is correctly recognized only in the context of the same task. (B) The probabilities obtained for the states in Figure 7A were processed with an argmax function in order to calculate the classification results plotted in confusion matrices. The rows correspond to the real labels (epochs free, delay and movement), the columns to predicted labels.